Physical Mechanism of p-i-n-Diode-Based Photonic Crystal Silicon Electrooptic Modulators for Gigahertz Operation

Lanlan Gu, Wei Jiang, Xiaonan Chen, and Ray T. Chen, *Fellow, IEEE*

***Abstract*—In this paper, the physical mechanism governing the optical modulation in a p-i-n-diode-embedded photonic crystal (PC) silicon Mach–Zehnder interferometer modulator is examined. Optical simulations have been performed to study how the slow group velocity of the photonic crystal waveguides enables a significant reduction of device size. The theoretical speed limitation in a PC-based silicon modulator is also explored. The 2-D semiconductor device simulator MEDICI has been employed to analyze the transient behavior of the p-i-n-diode-embedded silicon modulator. Electrical simulations have revealed a significant improvement in modulation speed upon the enhancement of current density in a downscaled PC device. High-speed optical modulation at 1 G $\cdot$ s^{-1} has been experimentally demonstrated. The performance degradation in optical modulation at the low-frequency operation region attributed to the thermooptic effect is identified and discussed. Simulations have also revealed that the modulation speed of our device can be improved up to 10 GHz by further reducing the device dimensions with little penalty of the increased optical loss.**

***Index Terms*—Optical modulation, photonic bandgap materials, silicon.**

I. Introduction

As THE CMOS technology continues to scale down, some physical limitations of conventional metal interconnects, such as bandwidth, power consumption, and crosstalk noise, have been the impetus for the investigation of optical interconnects. The global research interest on silicon photonics has increased rapidly in recent years. It has been trigged by the realization of cost-effect monolithic integration of the optical and electrical devices on a silicon platform, using the readily transferred very-large-scale-integrated (VLSI) technology. Significant progresses have been made for investigating silicon low-loss waveguides, light emitters, lasers, amplifiers, and photodetectors in the past few years, which promise an entry of silicon microphotonics interconnection at the hybrid, multichip level with migration to monolithic on-chip architectures [1]. Nevertheless, the development of all-silicon electrooptic modulators, a key optical interconnection component that encodes electrical information signals onto optical carriers, lags a little behind. Among a few standard approaches to realizing optical modulators, Mach–Zehnder interferometer (MZI), which converts a phase modulation to an amplitude modulation, is the most extensively studied type of modulator owing to its superior optical performance, such as high extinction ratio and large bandwidth of the operating wavelength. Relying on the facts that unstrained pure crystal silicon does not have linear electrooptic (pockels) effect, and other electrooptic effects such as the Kerr effect and Franz–Keldysh effect are extremely weak in silicon, the plasma (free carrier) dispersion effect is considered the most effective mechanism to obtain electrooptic modulation in silicon [2]. Plasma dispersion effect describes dependence of the refractive index on the free carrier concentration. The well-known empirical expression of the index perturbation versus the variation of free carrier concentration was developed by Soref and Bennett [2], which is given by

$$\Delta n = -[8.8 \times 10^{-22}\,\Delta N + 8.5 \times 10^{-18}\,(\Delta P)^{0.8}] \qquad (1)$$

where Δn is the refractive index change, and ΔN and ΔP are the variations of free carrier concentration for electrons and holes, respectively. Generally, long device length and slow switching speed are considered two major issues associated with the existing silicon MZI electrooptic modulators, as shown in Table I [3]–[13]. These long-standing problems stem from some of the intrinsic limitations of silicon material properties. Given the relatively low values of the mobility and long lifetime of both electrons and holes in silicon, the switching speed of silicon electrooptic modulators is usually slower than the inherently fast III–V-semiconductor-based devices. The weak response of silicon optical properties to the excitation of external fields, which can be understood, in the scenario of plasma effect, as the small variation of refractive index induced by the perturbation of free carrier, explains for the typically long device size of silicon MZIs. Therefore, innovative solutions have yet to be sought through creative device concepts and advanced technologies. Recently, the extension of a nanoapproach–photonic crystal (PC) approach to silicon photonics has brought revolutionary new opportunities to address these fundamental issues [8], [14], [15]. PCs are multidimensionally periodic dielectric structures, which enable the realization of novel and fascinating properties that are unattainable from naturally existing

Manuscript received November 29, 2007; revised March 22, 2008. This work was supported in part by the Air Force Office of Scientific Research under Grant FA9550-05-C-0171, in part by the National Science Foundation (NSF) National Nanotechnology Infrastructure Network (NNIN) Program, and in part by the Defence Advanced Research Project Agency (DARPA) AP2C Program.

L. Gu was with the Microelectronic Research Center, Department of Electrical and Computer Engineering, University of Texas, Austin TX 78758 USA. She is now with Omega Optics, Inc., Austin, TX 78758 USA (e-mail: lanlan.gu@omegaoptics.com).

W. Jiang was with the Omega Optics Inc., Austin, TX 78758 USA. He is now with the Department of Electrical and Computer Engineering, Rutgers University, Piscataway, NJ 08854 USA (e-mail: wjiangnj@ece.rutgers.edu).

X. Chen and R. T. Chen are with the Microelectronic Research Center, Department of Electrical and Computer Engineering, University of Texas, Austin, TX 78758 USA (e-mail: Xiaonan_chen@mail.utexas.edu; chen@ece.utexas.edu).

Color versions of one or more of the figures in this paper are available online at http://ieeexplore.ieee.org.

Digital Object Identifier 10.1109/JSTQE.2008.925769

TABLE I
SILICON MZI ELECTROOPTIC MODULATORS REPORTED IN THE LITERATURE

Year	Author	Electrical structure	Frequency bandwidth / Switching time	Length(μm)	
1991[3]	Treyz	p-i-n	50ns	500	Experimental demonstration
1995[4]	Zhao	p-i-n	200ns	816	
2000[5]	Dainesi	p-i-n	10MHz	1000	
2004[6]	Liu	MOS	1GHz	2500	
2005[7]	Liao	MOS	10GHz	3450	
2007[8]	Our device	PC p-i-n	1GHz	80	
1997[9]	Cutolo	BMFET	3.5ns	1000	Theoretical prediction
2003[10]	Irace	p-i-n	1GHz	3000	
2004[11]	Png	p-i-n	0.3ns	465	
2005[12]	Gan	p-i-n	20GHz	2500	
2005[13]	Gardes	p^+pnp^+	0.014ns	2500	
2007	Our device	PC p-i-n	0.077ns	80	

materials. By exploiting one of the unique properties, slow light effect that PC provides, we have successfully demonstrated a more than tenfold reduction in device length of a silicon MZI modulator [15]. More recently, we reported the first p-i-n-diode-embedded PC silicon modulator that reaches the gigahertz speed under a low driving voltage [8]. We also discussed the architectural design aspects of photonic crystal waveguide (PCW) modulators in our recent review paper [16]. In this paper, we provide a more detailed study to understand the physical mechanisms that cause such significant performance improvements regarding the device size, speed, and power consumption. In Section II, we present a simulation example of band structure calculation of a silicon PCW, which reveals how slow light effect benefits the miniaturization of silicon MZI modulators. In Section III, electrical simulation is performed to analyze the transient electrical behavior of a p-i-n-diode-embedded silicon modulator under forward bias condition. The considerable improvement in device speed attributed to the capability of downscaling device dimensions utilizing PCs is explored. Fabrication details of our device are presented in Section IV. Both optical and electrical characterizations are presented as well. In addition, the modulation degradation attributed to the thermooptic effect at the low-frequency operation region is observed and discussed.

II. OPTICAL SIMULATION

PCs, periodical dielectric structures composed of alternating dielectric materials with high and low refractive index, exhibit many unique optical characteristics. They thus promise to bring unprecedented opportunities for realizing large-scale, high-density photonic integrated circuits. With a sufficiently large refractive index contrast, a photonic bandgap, a forbidden frequency range in a certain direction for photons under a certain polarization, occurs [17]. It adds an additional guiding mechanism, which is different from the conventional index-contrast guiding mechanism, to realize optical waveguiding structure. A PCW is essentially a one-dimensional defect created inside

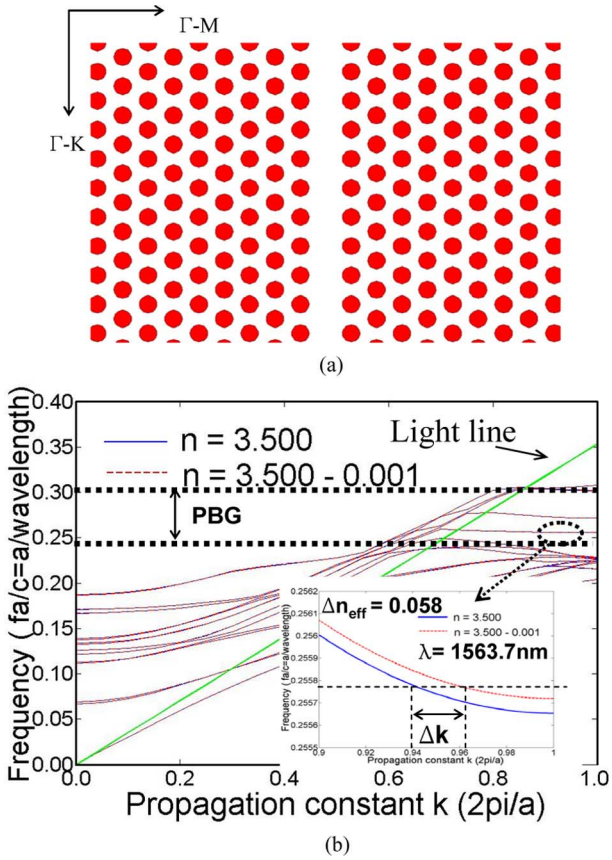

Fig. 1. (a) Drawing of hexagonal-lattice-based defect line PCW. (b) Dispersion curves of the defect-line silicon PCW with silicon refractive index of 3.500 (solid line) and 3.500–0.001 (dashed line).

a PC, which is most likely to introduce some guided mode bands within the photonic bandgap. It has been discovered that these guided mode bands always comprise a flat region near the boundary of the Brillouin zone. At the flat regions of such bands, the guided modes show extraordinary high dispersion or extremely small group velocity $(d\omega/dk)$, which allows a significant size reduction to be achieved in time-delay/phase-shift optical devices [8], [16]–[22].

Silicon is considered an ideal material to build PCW because it has a large index contrast with respect to air or silicon oxide, which is in favor of the formation of a photonic bandgap. To gain insight into how slow the group velocity can be obtained in a PCW, and in addition, how the slow group velocity influences the interaction length of MZI modulators, here we model the band structure of a carefully designed silicon line-defect PCW. The band diagram for TE-like wave in a silicon PC slab is simulated using the plane wave expansion method. A typical scenario that a silicon air–hole type PC slab is immersed in a low-dielectric material, such as polymer or silicon dioxide, is assumed. The thickness of silicon layer is assumed to be 230 nm. We also assume that refractive indexes of silicon and the low-dielectric material are 3.500 and 1.450, respectively. A defect-line PCW is generated by removing the central row of the low-dielectric material in the Γ–K direction of a hexagonal lattice, as illustrated in Fig. 1(a). The lattice constant and hole diameter of the PC structure are 400 and 220 nm, respectively. We use ten periods in a supercell of a PCW for the simulation. Fig. 1(b) shows two

sets of dispersion curves of the simulated structure. The green line is the light line of the silicon waveguide. There is no nonradiative guided mode existing in the region of the band diagram above the light line. The solid lines are calculated using silicon refractive index value (n) of 3.500 whereas the dashed lines are the calculation results for a small refractive index perturbation (Δn) of –0.001. A close look at the band structure reveals that some guided modes appear in a widely opened photonic bandgap if a line defect is introduced in the PC slab. One may note that the dispersion curves of these guided modes are rather flat around the edge of the Brillouin zone, which indicates an extremely small group velocity ($d\omega/dk$) of the defect mode in the region close to the band edge. As seen in the magnified view of this slow-group-velocity region, which is shown in the inset of Fig. 1(b), a small perturbation of the refractive index causes a slight vertical shift of the dispersion curve. And most importantly, such a small shift may lead to a huge variation of the wave vector (or the effective refractive index n_{eff}) of the guided mode. For example, given a fixed operation wavelength at 1536.7 nm, which is illustrated by the horizontal dotted line, a material refractive index change (Δn) of 0.001 generates a huge effective refractive index change (Δn_{eff}) of 0.058 for the simulated structure. In contrast, for conventional dielectric waveguides, Δn_{eff} is approximately equal to Δn. Such a significant amplification of Δn_{eff} in PCWs brings a tremendous impact on the scaling of the MZI modulators. It was well established that the required interaction length to obtain a π phase shift for a guided wave in MZI modulators is given by

$$L_\pi = \frac{\lambda}{2\Delta n_{\text{eff}}}. \tag{2}$$

As seen in (2), the required device length is inversely proportional to the effective refractive index change of the waveguide. Simulation results indicate that a length reduction by a few tens of times from the conventional device can be achieved if the simulated PCW structure replaces the conventional waveguide in the silicon MZI modulator.

III. Electrical Simulation

To achieve high-speed modulation in silicon modulators, it has been a big challenge for many years. Although earlier theoretical paper has predicted that the electrooptic effect enables gigahertz modulation in silicon MZI modulator, it was not until recently that Liu *et al*. first reported the experimental demonstration using a MOS-capacitor-based structure [6]. However, MOS modulators have a small overlap between the optical mode and the nonequilibrium carrier distribution. This could limit the modulation efficiency, resulting in a long device length to obtain a complete switching function. In contrast, p-i-n-diode-embedded structure enables an efficient electrooptic interaction through maximizing the overlap between the electrical field and optical field within the device active region. In comparison with the MOS-based structure, a few other advantages that the p-i-n-diode-embedded structure may bring include larger flexibility to integrate with optical waveguide and less complication in fabrication.

The limit of switching speed of a p-i-n diode is determined by carrier injection time (transit time) and carrier recombination time. As is seen in Table I, the switching speed that has been experimentally achieved for the conventional p-i-n-diode-based MZI modulator is far below 1 GHz. To discuss the possible reasons for its low-speed operation, one should understand the carrier transport mechanism within the p-i-n diode. The forward current flow j through a p-i-n diode is composed of the recombination current j_{i} of the excess carriers within the i-region and the diffusion currents $j_{\text{p}} + j_{\text{n}}$ in the heavily doped regions [23]. Consider scenarios involving medium or high current injection, where a high-level carrier injection is obtained in the middle of lightly doped intrinsic region but the injection level in heavily doped border region is still low, the contribution from $j_{\text{p}} + j_{\text{n}}$ to the whole current can be neglected [24] so that j is approximately equal to j_{i}. From charge control considerations $Q_{\text{i}} = It \sim jAt$, where Q_{i} is the total excess base charge in a diode of cross-sectional area A, the carrier injection time or the effective transit time of the diode t is given by

$$t = \frac{qW\Delta\bar{n}}{j} \tag{3}$$

where $\Delta\bar{n}$ is the average value of the carrier concentration in the quasineutral zone of the i-region and W is the width of the i-region. It is obvious that the carrier injection time can be reduced or the device speed can be increased by increasing the current density for a given carrier injection level and device dimension. A conventional p-i-n-diode-embedded MZI modulator requires large device dimensions, which is usually a few micrometers high, and several hundreds micrometers to several millimeters long. Operations at high current densities in such a device cause huge power consumption, and thus, are unsuitable for most on-chip optical interconnect applications. PC-based MZI is capable of shrinking the device height to hundreds of nanometers and interaction length to tens of micrometers, which provides at least twofold increase of the current density for the same level of current injection. Therefore, the miniaturization of MZI modulators brings a huge speed advantage for the turn-on process. Upon removal of forward bias, the excess carriers stored in the i-region decay by recombination to their thermal equilibrium value. For a turn-off process, the fall time or the recovery time is linearly proportional to the effective carrier lifetime, which can be expressed by

$$\frac{1}{\tau_{\text{eff}}} = \frac{1}{\tau_B} + \frac{1}{\tau_s} \tag{4}$$

where τ_B is the bulk recombination lifetime and τ_s is the surface recombination lifetime. The τ_{eff} of a conventional p-i-n-diode-based silicon MZI modulator is often determined by the bulk recombination, which is typically in a time range of submicroseconds to microseconds, because the surface effect can be ignored in devices with relatively large geometric dimensions. However, for our PC MZIs, the surface effect should be taken into account because the device thickness is reduced by more than one order of magnitude compared with the conventional device. More importantly, the ratio of actual surface area to bulk volume in a PC device is substantially increased attributed

to the introduction of arrayed hole or pillar structures into the device. Therefore, τ_{eff} of our device no longer bears any resemblance to τ_B and is most likely to be determined by surface recombination. If the silicon waveguide surfaces are not passivated, the surface recombination velocity could reach a very large value [25], which significantly reduces the τ_s and τ_{eff} correspondingly. In a practical circuit situation, the forward-biased diode can be turned off in an even shorter time than the effective carrier lifetime as the fall time t_{off} can be approximately related to τ_{eff} and electrical current by [23]:

$$t_{\text{off}} = \tau_{\text{eff}} \ln\left(1 + \frac{I_f}{I_r}\right) \tag{5}$$

where I_f is the forward current at the onstate and I_r is the transient reverse current during the initial recovery period of the offstate. It was reported that the time to extract excess electrons and holes can be reduced to tens of picoseconds in reverse-biased operation [26]. Upon the aforementioned discussion, one may reach a conclusion that the carrier injection time for the turn-on process, rather than the depletion time for the turn-off process, is the limiting factor that determines the switching speed of our p-i-n devices.

To further explore the carrier injection process of the proposed p-i-n devices, we have performed transient electrical analysis using a 2-D semiconductor device simulator MEDICI [27]. This simulator is a commercially available software that is widely used for similuiton, and this program has been employed to obtain the time-dependent carrier concentration distribution by solving the coupled Poisson's and charge continuity equations. Advanced physics device models are included in the program to enable an accurate estimation of the device properties. Unless otherwise stated, the structure simulated has the dimension shown in Fig. 2. The p-i-n diode is implemented on a silicon-on-insulator (SOI) wafer with the top silicon layer of 230 nm and the buried oxide layer of 2000 nm. Note that a thick buried oxide layer is chosen to ensure a sufficiently good optical confinement of silicon waveguides. Ideally, decreasing the width of i-region allows a shorter transit time, and consequently, faster turn-on speed. However, the heavily doped p^+ and n^+ border regions require to be sufficiently isolated from the optical field to avoid extra optical loss due to free carrier absorption. The width of i-region is thus assumed to be 4 μm as a compromise between the switching speed and optical loss. Width of the p^+ and n^+ regions is chosen to be 3 μm. The intrinsic region has an n-type background doping of 10^{15} cm^{-3}. A constant doping profile with a concentration of 5×10^{19} cm^{-3} is assumed for both p^+ and n^+ regions.

2-D time-dependent carrier distributions across the whole diode region upon the application of a forward turn-on voltage (V_{on}) of 0.89 V are simulated. As is verified by 2-D mapping, the electron and hole concentration profiles vary insignificantly with both depth and width, which leads to a uniform refractive index variation over the entire waveguiding region. An example of such a 2-D profile is shown in Fig. 3. The electron and hole concentration profiles at the half depth of the top silicon layer at various time points are plotted along the device lateral dimension, as shown in Fig. 4. Simulations reveal that the carrier injection into the intrinsic region reach a saturation level at 3×10^{17} cm^{-3} at 6.78 ns. It can be calculated using (1) that this injection level will change the refractive index by -0.001, which is considered a commonly targeted value to ensure a practical application [3]–[5], [8]–[10]. It must be noted that the turn-on process under this biasing condition is not fast enough

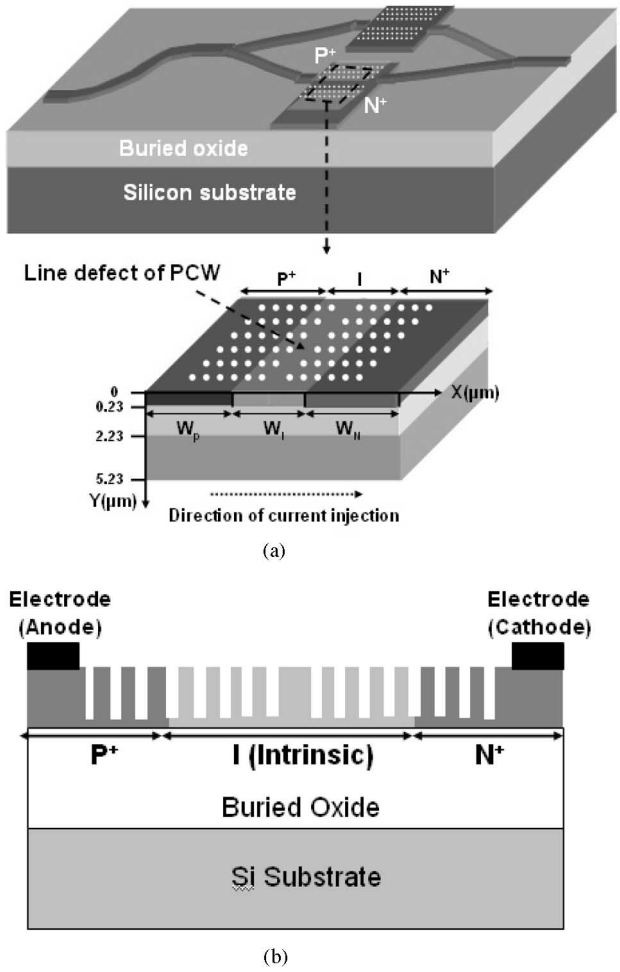

Fig. 2. Schematics of the PC silicon MZI modulator. (a) Perspective view. (b) Cross-sectional view.

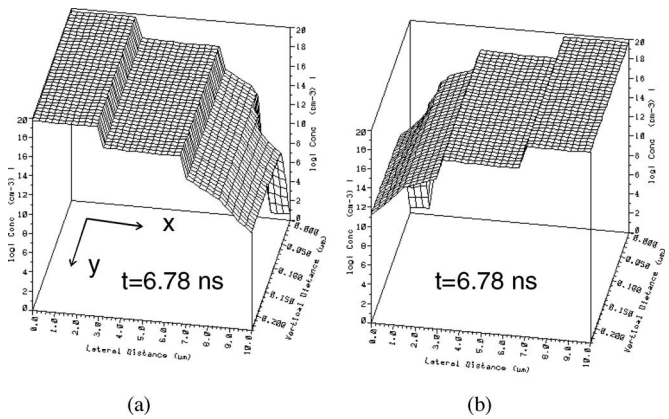

Fig. 3. 2-D (a) hole, and (b) electron concentration profiles at $t = 6.78$ ns under the forward biasing voltage at 0.89 V.

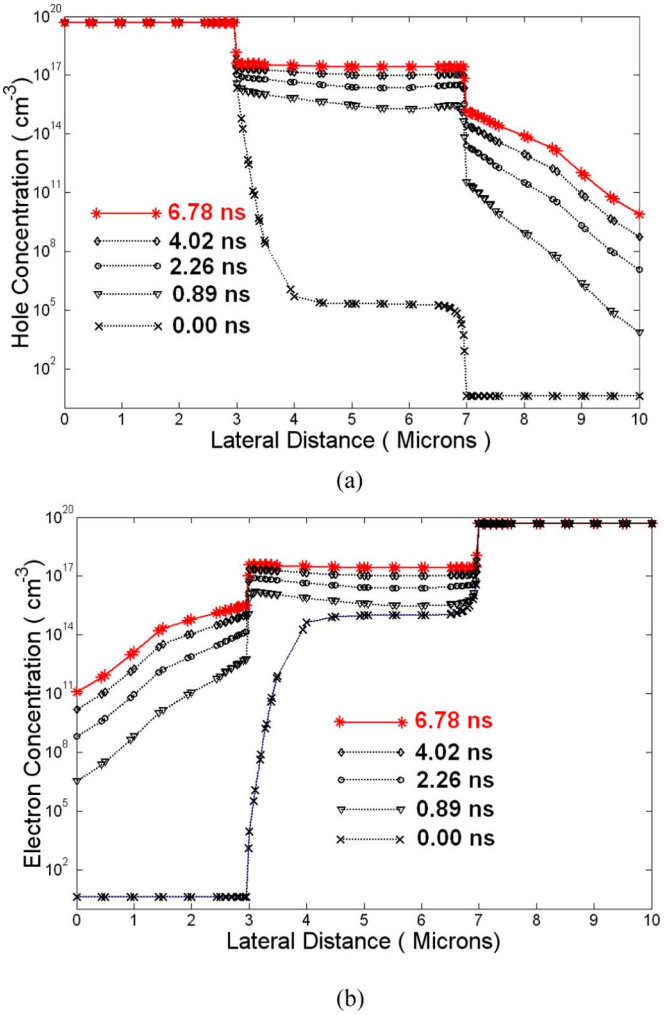

Fig. 4. Carrier concentration profiles at the half depth of the top silicon layer at various time points under the forward biasing voltage at 0.89 V. (a) Time-dependent hole concentration distribution. (b) Time-dependent electron concentration distribution.

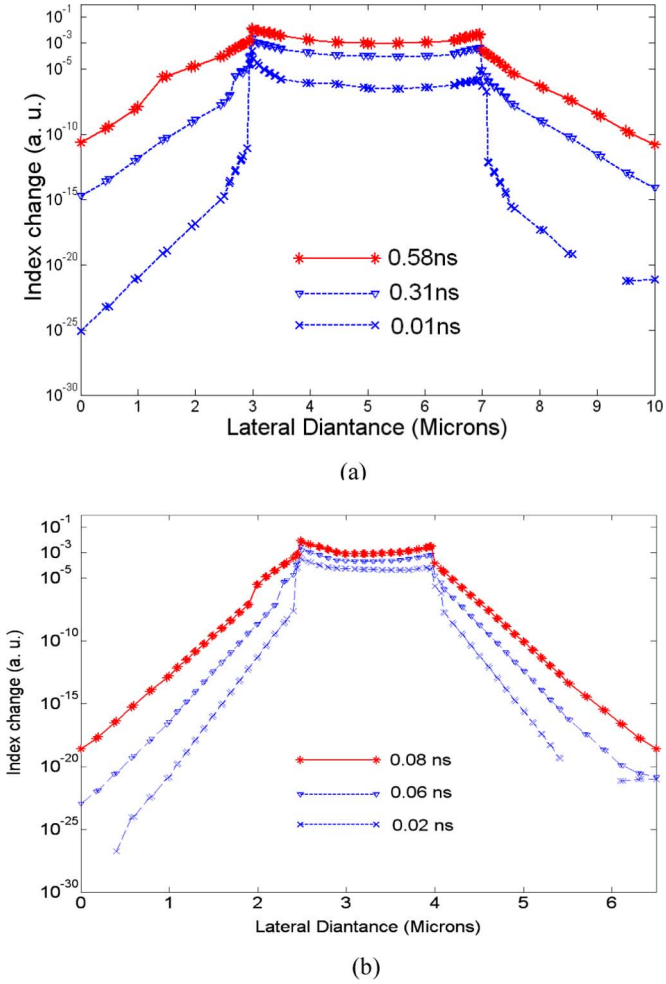

Fig. 5. Refractive index change along the lateral dimension of the p-i-n diode at the half depth of the top silicon layer under the forward biasing voltage at 2 V. (a) p-i-n diode with the intrinsic region of 4 μm. (b) p-i-n diode with the intrinsic region of 1.5 μm.

for gigahertz modulation. Recalling the discussion regarding the transit speed versus the current density in Section II, we have learned that the speed can be improved at a cost of higher current density. Given the fact that our devices are largely scaled down compared with the conventional devices, we are able to improve the speed by increasing the current density to a level such that the overall power consumption is still reasonably low for practical applications. A higher voltage of 2 V, which accordingly provides higher current density, is applied for the improvement of device speed. To obtain a more straightforward insight, variations of the free carrier concentration extracted from the simulation results were subsequently converted to the refractive index changes using (1). As is seen in Fig. 5(a), the targeted refractive index change of 0.001 (corresponding to an injection level of $3 \times 10^{17}\,\mathrm{cm}^{-3}$) has been reached within 0.58 ns under 2 V after switching on the p-i-n diode, which ensures the gigahertz modulation capability.

Reducing the width of the intrinsic region could be an efficient way to further increase the switching speed, whereas it may also cause extra optical loss depending on how large the overlap between the guided optical mode and the highly absorptive p^+ and n^+ regions is. Our earlier simulation revealed that the energy density drops by 20 dB at a distance of 0.75 μm away from the central line of PCW [22], which sets the lower limit of the separation distance between two highly doped regions at around 1.5 μm. The transient behavior of a 1.5-μm-wide p-i-n diode is simulated. Fig. 5(b) shows the corresponding time-dependent spatial change in the refractive index of the silicon core layer. A significant decrease in the carrier filling time is observed in this shrunk structure. Within 0.077 ns after turning on the device, a fairly uniform index change of 0.001 is attained over the entire intrinsic or waveguiding region. It gives another tenfold reduction of the switching speed from the 4-μm-wide device, pushing the modulation capability up to10 GHz. More importantly, with a given interaction length of a PC MZI, index changes smaller than 0.001 might be sufficient to ensure a complete switching function. It virtually depends on how much the enhancement of the group refractive index could be obtained in a specifically designed PC structure. In principle, an even faster switching speed can be achieved in a p-i-n-diode-embedded PC modulator if

deliberate efforts would be made in the band structure design of PCs.

IV. Experiments

Considering the complication of fabrication procedures, we built our silicon PC MZI modulator using the previously simulated 4-μm-wide structure. A wafer with the top silicon layer of 260 nm and a buried oxide layer of 2 μm was selected as the device substrate. A thermal oxide of about 80 nm, grown at 850 °C in H_2O atmosphere, served as an etching mask for silicon reactive ion etching (RIE). In addition, this thin oxide worked as a screen layer to minimize the channeling effect occurring in the ion implantation. The device structure using the previously simulated lattice parameters was defined by electron beam lithography. Device patterns were transferred to the oxide layer by RIE using CHF_3. The next step is to strip off the electron beam resist by a heated Pirahna (solution of sulfuric acid and hydrogen peroxide) cleaning. Following that, the device structure was defined on the silicon core layer by RIE to a depth of 230 nm using oxide as the hard mask. The windows for p^+ and n^+ implantation were opened by photolithography. Ion implantations of boron at 30 keV and phosphorus at 50 keV were performed to achieve an average doping concentration about 5×10^{19} cm^{-3} for highly doped p^+ and n^+ regions. The thermal rapid annealing for 1 m at 950° in a flowing nitrogen environment was performed afterwards to anneal the lattice defects and activate the implanted atoms. After that, electrode contact windows were opened by photolithography and the top thermal oxide inside the windows were removed. Aluminum electrodes were made by electron-beam evaporation and a subsequent lift-off process. Finally, a good ohmic contact between the aluminum electrodes and the underlying silicon was formed by sintering the device at a temperature of 400 °C for 30 min in a forming gas ambient. As the last step, an acrylate-based polymer layer was coated to cover the whole device. The microscopic image of the resulting device is shown in Fig. 6. To sustain high current density, care was taken to design the geometry of the highly doped regions and electrodes. For example, our initial experiments, in which the p^+ and n^+ regions in early fabricated samples were longer than the PCW, showed that the PC p-i-n diode tended to break down at the two ends of a PCW. This was identified to arise from highly concentrated electrical field, and the accompanying high electrical current density, localized at the PCW ends. Shortening p^+ and n^+ regions, as shown in Fig. 6, overcame this issue.

The I–V characteristic of the PC p-i-n diode was measured and the result is plotted in Fig. 7. Similar to the I–V dependence of the conventional p-i-n diode described by Shockley's and Hall's theories [24], the I–V relation $I \sim \exp(qV/k_BT)$ in the low-level injection region and $I \sim \exp(qV/2k_BT)$ in the high-level region are both observed, where V is the applied voltage, k_B is the Boltzmann's constant, and T is the temperature. This electrical characterization experimentally confirmed that the operation of our device, which was biased at 2 V for the turn-on state, run into a scenario of high-level current injection, where our theoretical analysis presented in Section IV is

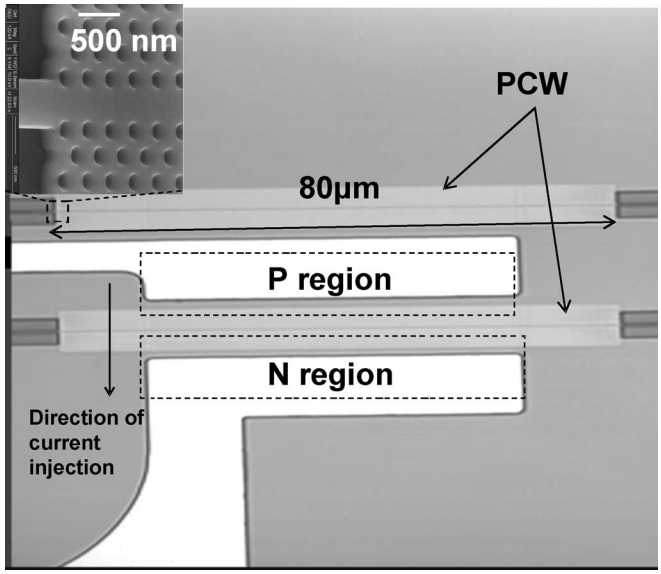

Fig. 6. Microscopic image of a p-i-n-diode-based PC MZI silicon modulator. The inset is the scanning electron microscopy image of the defect-line silicon PCW.

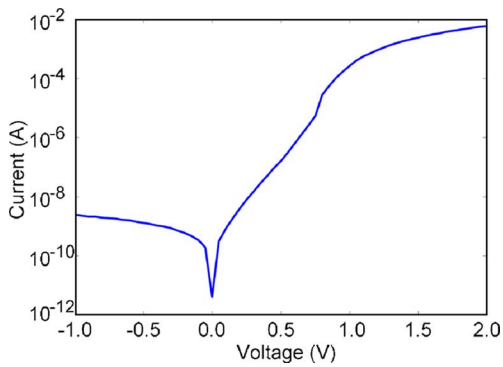

Fig. 7. I–V curve of the PC p-i-n.

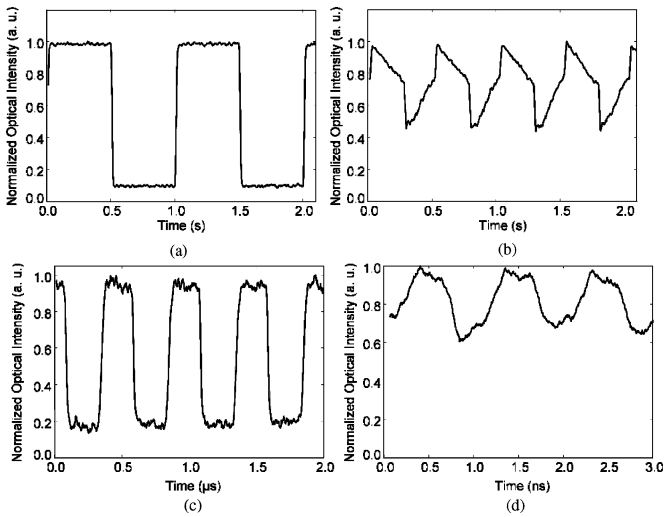

Fig. 8. Modulation traces at: (a) 1 Kb · s^{-1}. (b) 200 Kb · s^{-1}. (c) 2 Mb · s^{-1}. (d) 1 Gb · s^{-1}.

readily applied. We used TE-polarized light at a wavelength of 1541 nm, which is close to the transmission band edge of the defect mode, for the optical characterization. Lensed and tapered polarization maintaining fibers were used to couple the light into and out of the on-chip devices. An Agilent 8133 A pulse generator (up to 3 Gb $\cdot$ s^{-1}) was used to generate electrical driving signals. Modulated optical signals were detected by a 30-GHz photo detector that is internally integrated in the HP 83480 A digital communication analyzer. Square wave electrical signals at a peak-to-peak voltage of 3 V ($V_{\rm on} = 2\,{\rm V}, V_{\rm off} = -1\,{\rm V}$) with a duty cycle of 50% were used for the dynamic modulation characterization. Fig. 8 shows the optical modulation signals at various bit rates. It must be noted that the waveform of the modulated signal varies appreciably versus the modulation frequency. For the modulation at very low speed, the modulated signal reproduces the square wave of the driving signal perfectly, as shown in Fig. 8(a). A severe distortion of the waveform accompanied with the reduced modulation depth has been found in the modulated signal when the modulation speed increases to a few hundreds kilobits per second. Interestingly, good quality of modulation signals is regained when further increasing the modulation frequency up to a few megahertz. We believe that this phenomenon is related to the competition between the electrooptic and thermooptic effect that is inevitably involved in a current injection process. As current injection is always associated with power dissipation, the thermal effect of joule heating is always present in a current device. In contrast to the plasma effect, i.e., excess free carriers reduce the refractive index, temperature rise due to joule heating increases the refractive index. However, the thermal response is much slower than the electrical response. Typically, thermooptic effect cannot reach the frequency response beyond a few hundreds of kilohertz [28]. Consequently, it competes with the plasma dispersion effect in an opposite way for low-frequency modulations. The variation of the modulation trace versus frequency, shown in Fig. 8(a)–(d), delineates a clear transition from the thermal domination at low frequencies to plasma domination at high-frequency region. It is estimated that the temperature increase in our device under a forward operation is around 10°, which approximately leads to refractive index change of 0.002 in silicon. Therefore, the thermooptic effect dominates over the plasma effect at the low-frequency region. However, the thermal dominance starts getting weaker and weaker as the operation speed increases up to a few hundreds of kilohertz, the speed at which the thermal response can hardly keep pace with the electrical driving signal. An obvious degradation in the modulation at 200 Kb$\cdot$s^{-1}, a corner frequency of the thermal response region, has been observed, as shown in Fig. 8(b). As the frequency further increases to above a few megahertz, when the thermo-effect is no longer able to pick up such a fast switching speed, plasma effect starts to play a major role in the modulation mechanism. As is shown in Fig. 8(c), a square-wave modulation curve resembling the low-frequency signal appears when the frequency increases to 2 Mb $\cdot$ s^{-1}, which demonstrates the high-speed response of the electrooptic effect. Fig. 8(d) shows that the modulation depth is reduced by 3 dB as the modulation frequency further increases to 1 Gb $\cdot$ s^{-1}. The measured speed limit is in good agreement with the electrical simulation. To make electrooptic modulation more efficient, a good thermal heat sink has to be designed to minimize the competition from thermooptic effect. The demonstrated modulation above 2 Mb $\cdot$ s^{-1} is considered a pure electrooptic modulation. A reliable device performance at gigahertz operation frequency of our current device is readily achieved using especially designed high-speed drive circuitry. Further speed improvement can be achieved using the shrunk p-i-n diode we proposed earlier.

V. Conclusion

A p-i-n-diode-based PC silicon electrooptic MZI modulator has been proposed and fabricated. By incorporating PCWs into the MZI structure, device size has been reduced by more than one order of magnitude compared to the conventional devices. Optical simulation based on the plane-wave expansion method has been performed to reveal how slow group velocity in the silicon PCW dramatically increases the phase shift and thus reduces the size of the MZI modulator. We have performed electrical analyses to estimate device switching behavior by simulating time-dependent distributions of the carrier concentration. Simulations show that increasing current density under a given injection current by reducing the device size brings a huge speed advantage. The modulation capability above 10 GHz is predicted by shrinking the width of central intrinsic region of a p-i-n diode down to 1.5 μm. The high-speed electrooptic modulation at 1 Gb $\cdot$ s^{-1} has been experimentally demonstrated in a PC silicon MZI modulator within an interaction length of 80 μm. The inevitably involved thermooptic effect due to the high current injection is observed for modulations at low frequencies.

Acknowledgment

The devices were fabricated at UT Microelectronics Research Center.

References

[1] R. Soref, "Silicon photonics technology: Past, present, and future," *IEEE J. Sel. Topics Quantum Electron.*, vol. 12, no. 6, pp. 1678–1687, Nov./Dec. 2006.

[2] R. A. Soref and B. R. Bennett, "Electrooptical effects in silicon," *IEEE J. Quantum Electron.*, vol. QE-23, no. 1, pp. 123–129, Jan. 1987.

[3] G. V. Treyz, P. G. May, and J.-M. Halbout, "Silicon Mach–Zehnder waveguide interferometers based on the plasma dispersion effect," *Appl. Phys. Lett.*, vol. 59, pp. 77–773, 1991.

[4] C. Z. Zhao, G. Z. Li, E. K. Liu, Y. Gao, and X. D. Liu, "Silicon on insulator Mach–Zehnder waveguide interferometers operating at 1.3 μm," *Appl. Phys. Lett.*, vol. 67, pp. 2448–2451, 1995.

[5] P. Dainesi, A. Kung, M. Chabloz, A. Lagos, Ph. Fluckiger, A. Ionescu, P. Fazan, M. Declerq, Ph. Renaud, and Ph. Robert, "CMOS compatible fully integrated Mach–Zehnder interferometer in SOI technology," *Photon. Technol. Lett.*, vol. 12, no. 6, pp. 660–662, Jun. 2000.

[6] A. Liu, R. Jones, L. Liao, D. S. Rublo, D. Rubin, O. Cohen, R. Nicolaescu, and M. Paniccia, "A high-speed silicon optical modulator based on a metal-oxide-semiconductor capacitor," *Nature*, vol. 427, pp. 615–617, 2004.

[7] L. Liao, D. Samara-Rubio, M. Morse, A. Liu, D. Hodge, D. Rubin, U. D. Keil, and T. Franck, "High speed silicon Mach–Zehnder modulator," *Opt. Exp.*, vol. 13, pp. 3129–3135, 2005.

[8] L. Gu, W. Jiang, X. Chen, L. Wang, and R. T. Chen, "High speed silicon photonic crystal waveguide modulator for low voltage operation," *Appl. Phys. Lett.*, vol. 90, pp. 071105-1–071105-3, 2007.

[9] A. Cutolo, M. Iodice, P. Spirito, and L. Zeni, "Silicon electro-optic modulator based on a three terminal device integrated in a low-loss single-mode SOI waveguide," *J. Lightw. Technol.*, vol. 15, no. 3, pp. 505–518, Mar. 1997.
[10] A. Irace, G. Breglio, and A. Cutolo, "All-silicon optoelectronic modulator with 1 GHz switching capability," *Electron. Lett.*, vol. 39, pp. 232–233, 2003.
[11] C. E. Png, S. P. Chan, S. T. Lim, and G. T. Reed, "Optical phase modulator for MHz and GHz modulation in silicon-on-insulator (SOI)," *J. Lightw. Technol.*, vol. 22, no. 6, pp. 1573–1582, Jun. 2004.
[12] F. Gan and F. X. Kartner, "High-speed silicon electrooptic modulator design," *IEEE Photon. Technol. Lett.*, vol. 17, no. 5, pp. 1007–1009, May 2005.
[13] F. Y. Gardes, G. T. Reed, and N. G. Emerson, "A sub-micron depletion-type photonic modulator in silicon on insulator," *Opt. Exp.*, vol. 13, pp. 8845–8853, 2005.
[14] Y. A. Vlasov, M. O'Boyle, H. F. Hamann, and S. J. McNab, "Active control of slow light on a chip with photonic crystal waveguides," *Nature*, vol. 438, pp. 65–69, 2005.
[15] Y. Jiang, W. Jiang, L. Gu, X. Chen, and R. T. Chen, "80-micron interaction length silicon photonic crystal waveguide modulator," *Appl. Phys. Lett.*, vol. 87, pp. 221105-1–221105-2, 2005.
[16] W. Jiang, L. Gu, X. Chen, and R. T. Chen, "Photonic crystal waveguide modulators for silicon photonics: Device physics and some recent progress," *Solid-State Electron.*, vol. 51, pp. 1278–1286, 2007.
[17] J. D. Joannopoulos, R. D. Meade, and J. Winn, *Photonic Crystals*. Princeton, NJ: Princeton Univ. Press, 1995.
[18] M. Notomi, K. Yamada, A. Shinya, J. Takahashi, C. Takahashi, and I. Yokohama, "Extremely large group-velocity dispersion of line-defect waveguides in photonic crystal slabs," *Phys. Rev. Lett.*, vol. 87, pp. 253902-1–253902-4, 2001.
[19] M. Soljacic, S. G. Johson, S. Fan, M. Ibanescu, E. Ippen, and J. D. Joannopoulos, "Photonic-crystal slow-light enhancement of nonlinear phase sensitivity," *J. Opt. Soc. Amer. B*, vol. 19, pp. 2052–2059, 2002.
[20] T. Baba, A. Motegi, T. Iwai, N. Fukaya, Y. Watanabe, and A. Sakai, "Light propagation characteristics of straight single-line-defect waveguides in photonic crystal slabs fabricated into a silicon-on-insulator substrate," *IEEE J. Quantum Electron.*, vol. 38, no. 7, pp. 743–752, Jul. 2002.
[21] M. L. Povinelli, S. G. Johnson, and J. D. Joannopoulos, "Slow-light, band-edge waveguides for tunable time delays," *Opt. Exp.*, vol. 13, pp. 7145–7159, 2005.
[22] L. Gu, Y. Jiang, W. Jiang, X. Chen, and R. T. Chen, "Silicon-on-insulator-based photonic-crystal Mach–Zehnder interferometers," *Proc. SPIE*, vol. 6128, pp. 261–268, 2006.
[23] X. Ghandi, *Semiconductor Power Devices*. New York: Wiley, 1977.
[24] A. Herlet, "The forward characteristic of silicon power rectifiers at high current densities," *Solid-State Electron.*, vol. 11, pp. 717–742, 1968.
[25] C. A. Barrios, V. Almeida, and M. Lipson, "Low-power-consumption short-length and high-modulation-depth silicon eletrooptic modulator," *J. Lightw. Technol.*, vol. 21, no. 4, pp. 1089–1098, Apr. 2003.
[26] J. Muller, "Thin silicon film p-i-n photodiodes with internal reflection," *IEEE J. Solid-State Circuts*, vol. SSC-13, no. 1, pp. 173–179, Feb. 1978.
[27] *MEDICI User's Manual*, TMA Inc., Palo Alto, CA, 1992.
[28] G. Cocorullo, M. Iodice, I. Rendina, and P. M. Sarro, "Silicon thermo-optical micro-modulator with 700 kHz-3 dB bandwidth," *IEEE Photon. Technol. Lett.*, vol. 7, no. 4, pp. 363–365, Apr. 1995.

Lanlan Gu received the B.S. and M.S. degrees in physics from Fudan University, Shanghai, China, in 1998, and 2001, respectively, and the Ph.D. degree in electrical and computer engineering from the University of Texas, Austin, in 2007.

She is currently a Research Scientist with Omega Optics, Inc., where she is involved in electrooptic laser beam steering and light emitting devices. Her current research interests include a variety of topics in the areas of optical communications and optical interconnects, which extend from free-space diffractive optical elements to integrated photonic devices. She has authored or coauthored over 40 publications in refereed journals and conferences.

Wei Jiang received the B.S. degree in physics from Nanjing University, Nanjing, China, in 1996, and the M.A. degree in physics and the Ph.D. degree in electrical and computer engineering from the University of Texas, Austin, in 2000 and 2005, respectively.

Since 2007, he has been an Assistant Professor in the Department of Electrical and Computer Engineering, Rutgers University, Piscataway, NJ. His current research interests include the intersection of nanotechnology and photonics with current emphasis on photonic crystals, silicon photonics, optical interconnects, and beam steering.

Xiaonan Chen received the B.S. degree in precision instruments and mechanology from Tsinghua University, Beijing, China, in 2002, and the M.S. degree in electrical and computer engineering from the University of Texas, Austin, in 2006, where he is currently working toward the Ph.D. degree at the Microelectronics Research Center.

Ray T. Chen (M'91–SM'98–F'04) received the B.S. degree in physics from the National Tsing-Hua University, Hsinchu, Taiwan, in 1980, and the M.S. degree in physics and the Ph.D. degree in electrical engineering from the University of California (UC), Berkeley, in 1983 and 1988, respectively.

From 1988 to 1992, he was a Research Scientist, a Manager, and the Director of the Department of Electrooptic Engineering, Physical Optics Corporation, Torrance, CA. During 1992, he was engaged to start optical interconnect research program as a Faculty Member in the Department of Electrical and Computer Engineering (ECE), University of Texas (UT), Austin, where his group reported its research findings in more than 420 published papers including over 55 invited papers. He holds 12 issued patents. His current research interests include nanophotonic passive and active devices for optical interconnect applications, polymer-based guided wave optical interconnection and packaging, and true time delay (TTD) wideband phased array antenna (PAA). He has edited or coedited over 18 conference proceedings.

Dr. Chen is a Fellow of the Optical Society of America (OSA) and the International Society for Optical Engineers (SPIE). He was the recipient of the 1987 UC Regent's Dissertation Fellowship and the 1999 UT Engineering Foundation Faculty Award for his contributions in research, teaching, and services.

Physical Mechanism of p-i-n-Diode-Based Photonic Crystal Silicon Electrooptic Modulators for Gigahertz Operation

Lanlan Gu, Wei Jiang, Xiaonan Chen, and Ray T. Chen, *Fellow, IEEE*

***Abstract*—In this paper, the physical mechanism governing the optical modulation in a p-i-n-diode-embedded photonic crystal (PC) silicon Mach–Zehnder interferometer modulator is examined. Optical simulations have been performed to study how the slow group velocity of the photonic crystal waveguides enables a significant reduction of device size. The theoretical speed limitation in a PC-based silicon modulator is also explored. The 2-D semiconductor device simulator MEDICI has been employed to analyze the transient behavior of the p-i-n-diode-embedded silicon modulator. Electrical simulations have revealed a significant improvement in modulation speed upon the enhancement of current density in a downscaled PC device. High-speed optical modulation at 1 G $\cdot$ s^{-1} has been experimentally demonstrated. The performance degradation in optical modulation at the low-frequency operation region attributed to the thermooptic effect is identified and discussed. Simulations have also revealed that the modulation speed of our device can be improved up to 10 GHz by further reducing the device dimensions with little penalty of the increased optical loss.**

***Index Terms*—Optical modulation, photonic bandgap materials, silicon.**

I. Introduction

As THE CMOS technology continues to scale down, some physical limitations of conventional metal interconnects, such as bandwidth, power consumption, and crosstalk noise, have been the impetus for the investigation of optical interconnects. The global research interest on silicon photonics has increased rapidly in recent years. It has been trigged by the realization of cost-effect monolithic integration of the optical and electrical devices on a silicon platform, using the readily transferred very-large-scale-integrated (VLSI) technology. Significant progresses have been made for investigating silicon low-loss waveguides, light emitters, lasers, amplifiers, and photodetectors in the past few years, which promise an entry of silicon microphotonics interconnection at the hybrid, multichip level with migration to monolithic on-chip architectures [1]. Nevertheless, the development of all-silicon electrooptic modulators, a key optical interconnection component that encodes electrical information signals onto optical carriers, lags a little behind. Among a few standard approaches to realizing optical modulators, Mach–Zehnder interferometer (MZI), which converts a phase modulation to an amplitude modulation, is the most extensively studied type of modulator owing to its superior optical performance, such as high extinction ratio and large bandwidth of the operating wavelength. Relying on the facts that unstrained pure crystal silicon does not have linear electrooptic (pockels) effect, and other electrooptic effects such as the Kerr effect and Franz–Keldysh effect are extremely weak in silicon, the plasma (free carrier) dispersion effect is considered the most effective mechanism to obtain electrooptic modulation in silicon [2]. Plasma dispersion effect describes dependence of the refractive index on the free carrier concentration. The well-known empirical expression of the index perturbation versus the variation of free carrier concentration was developed by Soref and Bennett [2], which is given by

$$\Delta n = -[8.8 \times 10^{-22}\,\Delta N + 8.5 \times 10^{-18}\,(\Delta P)^{0.8}] \qquad (1)$$

where Δn is the refractive index change, and ΔN and ΔP are the variations of free carrier concentration for electrons and holes, respectively. Generally, long device length and slow switching speed are considered two major issues associated with the existing silicon MZI electrooptic modulators, as shown in Table I [3]–[13]. These long-standing problems stem from some of the intrinsic limitations of silicon material properties. Given the relatively low values of the mobility and long lifetime of both electrons and holes in silicon, the switching speed of silicon electrooptic modulators is usually slower than the inherently fast III–V-semiconductor-based devices. The weak response of silicon optical properties to the excitation of external fields, which can be understood, in the scenario of plasma effect, as the small variation of refractive index induced by the perturbation of free carrier, explains for the typically long device size of silicon MZIs. Therefore, innovative solutions have yet to be sought through creative device concepts and advanced technologies. Recently, the extension of a nanoapproach–photonic crystal (PC) approach to silicon photonics has brought revolutionary new opportunities to address these fundamental issues [8], [14], [15]. PCs are multidimensionally periodic dielectric structures, which enable the realization of novel and fascinating properties that are unattainable from naturally existing

Manuscript received November 29, 2007; revised March 22, 2008. This work was supported in part by the Air Force Office of Scientific Research under Grant FA9550-05-C-0171, in part by the National Science Foundation (NSF) National Nanotechnology Infrastructure Network (NNIN) Program, and in part by the Defence Advanced Research Project Agency (DARPA) AP2C Program.

L. Gu was with the Microelectronic Research Center, Department of Electrical and Computer Engineering, University of Texas, Austin TX 78758 USA. She is now with Omega Optics, Inc., Austin, TX 78758 USA (e-mail: lanlan.gu@omegaoptics.com).

W. Jiang was with the Omega Optics Inc., Austin, TX 78758 USA. He is now with the Department of Electrical and Computer Engineering, Rutgers University, Piscataway, NJ 08854 USA (e-mail: wjiangnj@ece.rutgers.edu).

X. Chen and R. T. Chen are with the Microelectronic Research Center, Department of Electrical and Computer Engineering, University of Texas, Austin, TX 78758 USA (e-mail: Xiaonan_chen@mail.utexas.edu; chen@ece.utexas.edu).

Color versions of one or more of the figures in this paper are available online at http://ieeexplore.ieee.org.

Digital Object Identifier 10.1109/JSTQE.2008.925769

TABLE I
SILICON MZI ELECTROOPTIC MODULATORS REPORTED IN THE LITERATURE

Year	Author	Electrical structure	Frequency bandwidth / Switching time	Length(μm)	
1991[3]	Treyz	p-i-n	50ns	500	Experimental demonstration
1995[4]	Zhao	p-i-n	200ns	816	
2000[5]	Dainesi	p-i-n	10MHz	1000	
2004[6]	Liu	MOS	1GHz	2500	
2005[7]	Liao	MOS	10GHz	3450	
2007[8]	Our device	PC p-i-n	1GHz	80	
1997[9]	Cutolo	BMFET	3.5ns	1000	Theoretical prediction
2003[10]	Irace	p-i-n	1GHz	3000	
2004[11]	Png	p-i-n	0.3ns	465	
2005[12]	Gan	p-i-n	20GHz	2500	
2005[13]	Gardes	p^+pnp^+	0.014ns	2500	
2007	Our device	PC p-i-n	0.077ns	80	

materials. By exploiting one of the unique properties, slow light effect that PC provides, we have successfully demonstrated a more than tenfold reduction in device length of a silicon MZI modulator [15]. More recently, we reported the first p-i-n-diode-embedded PC silicon modulator that reaches the gigahertz speed under a low driving voltage [8]. We also discussed the architectural design aspects of photonic crystal waveguide (PCW) modulators in our recent review paper [16]. In this paper, we provide a more detailed study to understand the physical mechanisms that cause such significant performance improvements regarding the device size, speed, and power consumption. In Section II, we present a simulation example of band structure calculation of a silicon PCW, which reveals how slow light effect benefits the miniaturization of silicon MZI modulators. In Section III, electrical simulation is performed to analyze the transient electrical behavior of a p-i-n-diode-embedded silicon modulator under forward bias condition. The considerable improvement in device speed attributed to the capability of downscaling device dimensions utilizing PCs is explored. Fabrication details of our device are presented in Section IV. Both optical and electrical characterizations are presented as well. In addition, the modulation degradation attributed to the thermooptic effect at the low-frequency operation region is observed and discussed.

II. OPTICAL SIMULATION

PCs, periodical dielectric structures composed of alternating dielectric materials with high and low refractive index, exhibit many unique optical characteristics. They thus promise to bring unprecedented opportunities for realizing large-scale, high-density photonic integrated circuits. With a sufficiently large refractive index contrast, a photonic bandgap, a forbidden frequency range in a certain direction for photons under a certain polarization, occurs [17]. It adds an additional guiding mechanism, which is different from the conventional index-contrast guiding mechanism, to realize optical waveguiding structure. A PCW is essentially a one-dimensional defect created inside

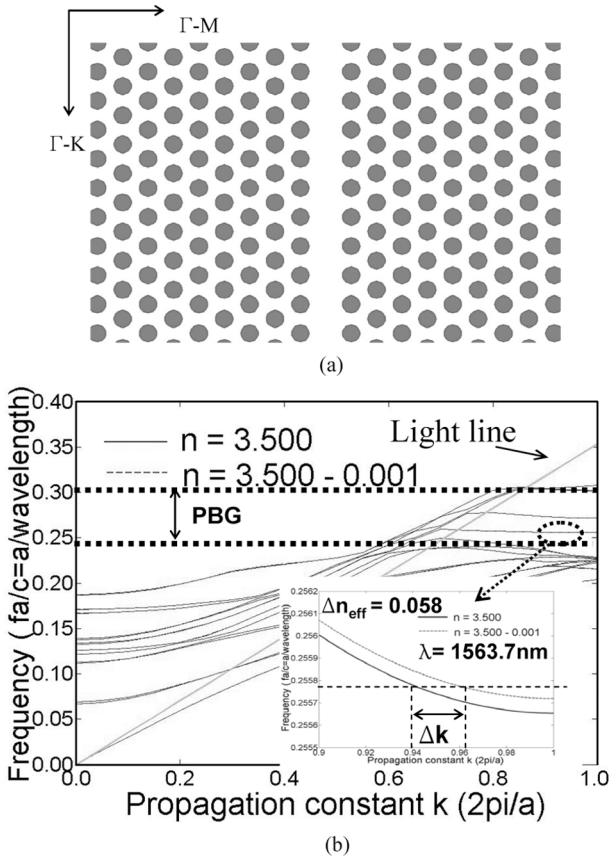

Fig. 1. (a) Drawing of hexagonal-lattice-based defect line PCW. (b) Dispersion curves of the defect-line silicon PCW with silicon refractive index of 3.500 (solid line) and 3.500–0.001 (dashed line).

a PC, which is most likely to introduce some guided mode bands within the photonic bandgap. It has been discovered that these guided mode bands always comprise a flat region near the boundary of the Brillouin zone. At the flat regions of such bands, the guided modes show extraordinary high dispersion or extremely small group velocity $(d\omega/dk)$, which allows a significant size reduction to be achieved in time-delay/phase-shift optical devices [8], [16]–[22].

Silicon is considered an ideal material to build PCW because it has a large index contrast with respect to air or silicon oxide, which is in favor of the formation of a photonic bandgap. To gain insight into how slow the group velocity can be obtained in a PCW, and in addition, how the slow group velocity influences the interaction length of MZI modulators, here we model the band structure of a carefully designed silicon line-defect PCW. The band diagram for TE-like wave in a silicon PC slab is simulated using the plane wave expansion method. A typical scenario that a silicon air–hole type PC slab is immersed in a low-dielectric material, such as polymer or silicon dioxide, is assumed. The thickness of silicon layer is assumed to be 230 nm. We also assume that refractive indexes of silicon and the low-dielectric material are 3.500 and 1.450, respectively. A defect-line PCW is generated by removing the central row of the low-dielectric material in the Γ–K direction of a hexagonal lattice, as illustrated in Fig. 1(a). The lattice constant and hole diameter of the PC structure are 400 and 220 nm, respectively. We use ten periods in a supercell of a PCW for the simulation. Fig. 1(b) shows two

sets of dispersion curves of the simulated structure. The green line is the light line of the silicon waveguide. There is no nonradiative guided mode existing in the region of the band diagram above the light line. The solid lines are calculated using silicon refractive index value (n) of 3.500 whereas the dashed lines are the calculation results for a small refractive index perturbation (Δn) of –0.001. A close look at the band structure reveals that some guided modes appear in a widely opened photonic bandgap if a line defect is introduced in the PC slab. One may note that the dispersion curves of these guided modes are rather flat around the edge of the Brillouin zone, which indicates an extremely small group velocity ($d\omega/dk$) of the defect mode in the region close to the band edge. As seen in the magnified view of this slow-group-velocity region, which is shown in the inset of Fig. 1(b), a small perturbation of the refractive index causes a slight vertical shift of the dispersion curve. And most importantly, such a small shift may lead to a huge variation of the wave vector (or the effective refractive index n_{eff}) of the guided mode. For example, given a fixed operation wavelength at 1536.7 nm, which is illustrated by the horizontal dotted line, a material refractive index change (Δn) of 0.001 generates a huge effective refractive index change (Δn_{eff}) of 0.058 for the simulated structure. In contrast, for conventional dielectric waveguides, Δn_{eff} is approximately equal to Δn. Such a significant amplification of Δn_{eff} in PCWs brings a tremendous impact on the scaling of the MZI modulators. It was well established that the required interaction length to obtain a π phase shift for a guided wave in MZI modulators is given by

$$L_\pi = \frac{\lambda}{2\Delta n_{\text{eff}}}. \tag{2}$$

As seen in (2), the required device length is inversely proportional to the effective refractive index change of the waveguide. Simulation results indicate that a length reduction by a few tens of times from the conventional device can be achieved if the simulated PCW structure replaces the conventional waveguide in the silicon MZI modulator.

III. Electrical Simulation

To achieve high-speed modulation in silicon modulators, it has been a big challenge for many years. Although earlier theoretical paper has predicted that the electrooptic effect enables gigahertz modulation in silicon MZI modulator, it was not until recently that Liu *et al*. first reported the experimental demonstration using a MOS-capacitor-based structure [6]. However, MOS modulators have a small overlap between the optical mode and the nonequilibrium carrier distribution. This could limit the modulation efficiency, resulting in a long device length to obtain a complete switching function. In contrast, p-i-n-diode-embedded structure enables an efficient electrooptic interaction through maximizing the overlap between the electrical field and optical field within the device active region. In comparison with the MOS-based structure, a few other advantages that the p-i-n-diode-embedded structure may bring include larger flexibility to integrate with optical waveguide and less complication in fabrication.

The limit of switching speed of a p-i-n diode is determined by carrier injection time (transit time) and carrier recombination time. As is seen in Table I, the switching speed that has been experimentally achieved for the conventional p-i-n-diode-based MZI modulator is far below 1 GHz. To discuss the possible reasons for its low-speed operation, one should understand the carrier transport mechanism within the p-i-n diode. The forward current flow j through a p-i-n diode is composed of the recombination current j_{i} of the excess carriers within the i-region and the diffusion currents $j_{\text{p}} + j_{\text{n}}$ in the heavily doped regions [23]. Consider scenarios involving medium or high current injection, where a high-level carrier injection is obtained in the middle of lightly doped intrinsic region but the injection level in heavily doped border region is still low, the contribution from $j_{\text{p}} + j_{\text{n}}$ to the whole current can be neglected [24] so that j is approximately equal to j_{i}. From charge control considerations $Q_{\text{i}} = It \sim jAt$, where Q_{i} is the total excess base charge in a diode of cross-sectional area A, the carrier injection time or the effective transit time of the diode t is given by

$$t = \frac{qW\Delta\bar{n}}{j} \tag{3}$$

where $\Delta\bar{n}$ is the average value of the carrier concentration in the quasineutral zone of the i-region and W is the width of the i-region. It is obvious that the carrier injection time can be reduced or the device speed can be increased by increasing the current density for a given carrier injection level and device dimension. A conventional p-i-n-diode-embedded MZI modulator requires large device dimensions, which is usually a few micrometers high, and several hundreds micrometers to several millimeters long. Operations at high current densities in such a device cause huge power consumption, and thus, are unsuitable for most on-chip optical interconnect applications. PC-based MZI is capable of shrinking the device height to hundreds of nanometers and interaction length to tens of micrometers, which provides at least twofold increase of the current density for the same level of current injection. Therefore, the miniaturization of MZI modulators brings a huge speed advantage for the turn-on process. Upon removal of forward bias, the excess carriers stored in the i-region decay by recombination to their thermal equilibrium value. For a turn-off process, the fall time or the recovery time is linearly proportional to the effective carrier lifetime, which can be expressed by

$$\frac{1}{\tau_{\text{eff}}} = \frac{1}{\tau_B} + \frac{1}{\tau_s} \tag{4}$$

where τ_B is the bulk recombination lifetime and τ_s is the surface recombination lifetime. The τ_{eff} of a conventional p-i-n-diode-based silicon MZI modulator is often determined by the bulk recombination, which is typically in a time range of submicroseconds to microseconds, because the surface effect can be ignored in devices with relatively large geometric dimensions. However, for our PC MZIs, the surface effect should be taken into account because the device thickness is reduced by more than one order of magnitude compared with the conventional device. More importantly, the ratio of actual surface area to bulk volume in a PC device is substantially increased attributed

to the introduction of arrayed hole or pillar structures into the device. Therefore, τ_{eff} of our device no longer bears any resemblance to τ_B and is most likely to be determined by surface recombination. If the silicon waveguide surfaces are not passivated, the surface recombination velocity could reach a very large value [25], which significantly reduces the τ_s and τ_{eff} correspondingly. In a practical circuit situation, the forward-biased diode can be turned off in an even shorter time than the effective carrier lifetime as the fall time t_{off} can be approximately related to τ_{eff} and electrical current by [23]:

$$t_{\text{off}} = \tau_{\text{eff}} \ln\left(1 + \frac{I_f}{I_r}\right) \tag{5}$$

where I_f is the forward current at the onstate and I_r is the transient reverse current during the initial recovery period of the offstate. It was reported that the time to extract excess electrons and holes can be reduced to tens of picoseconds in reverse-biased operation [26]. Upon the aforementioned discussion, one may reach a conclusion that the carrier injection time for the turn-on process, rather than the depletion time for the turn-off process, is the limiting factor that determines the switching speed of our p-i-n devices.

To further explore the carrier injection process of the proposed p-i-n devices, we have performed transient electrical analysis using a 2-D semiconductor device simulator MEDICI [27]. This simulator is a commercially available software that is widely used for similuiton, and this program has been employed to obtain the time-dependent carrier concentration distribution by solving the coupled Poisson's and charge continuity equations. Advanced physics device models are included in the program to enable an accurate estimation of the device properties. Unless otherwise stated, the structure simulated has the dimension shown in Fig. 2. The p-i-n diode is implemented on a silicon-on-insulator (SOI) wafer with the top silicon layer of 230 nm and the buried oxide layer of 2000 nm. Note that a thick buried oxide layer is chosen to ensure a sufficiently good optical confinement of silicon waveguides. Ideally, decreasing the width of i-region allows a shorter transit time, and consequently, faster turn-on speed. However, the heavily doped p^+ and n^+ border regions require to be sufficiently isolated from the optical field to avoid extra optical loss due to free carrier absorption. The width of i-region is thus assumed to be 4 μm as a compromise between the switching speed and optical loss. Width of the p^+ and n^+ regions is chosen to be 3 μm. The intrinsic region has an n-type background doping of 10^{15} cm^{-3}. A constant doping profile with a concentration of 5×10^{19} cm^{-3} is assumed for both p^+ and n^+ regions.

2-D time-dependent carrier distributions across the whole diode region upon the application of a forward turn-on voltage (V_{on}) of 0.89 V are simulated. As is verified by 2-D mapping, the electron and hole concentration profiles vary insignificantly with both depth and width, which leads to a uniform refractive index variation over the entire waveguiding region. An example of such a 2-D profile is shown in Fig. 3. The electron and hole concentration profiles at the half depth of the top silicon layer at various time points are plotted along the device lateral dimension, as shown in Fig. 4. Simulations reveal that the carrier injection into the intrinsic region reach a saturation level at 3×10^{17} cm^{-3} at 6.78 ns. It can be calculated using (1) that this injection level will change the refractive index by -0.001, which is considered a commonly targeted value to ensure a practical application [3]–[5], [8]–[10]. It must be noted that the turn-on process under this biasing condition is not fast enough

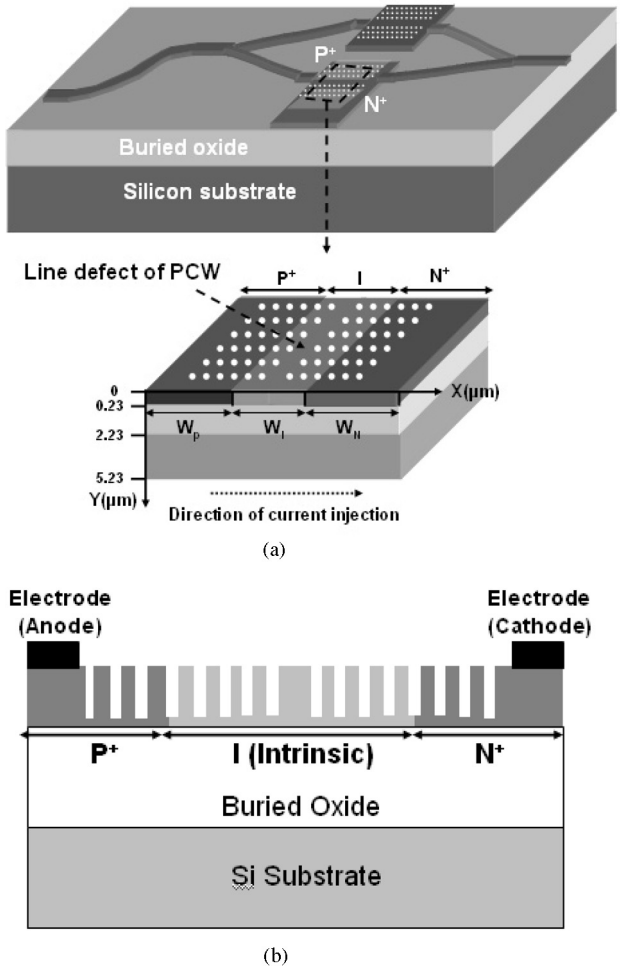

Fig. 2. Schematics of the PC silicon MZI modulator. (a) Perspective view. (b) Cross-sectional view.

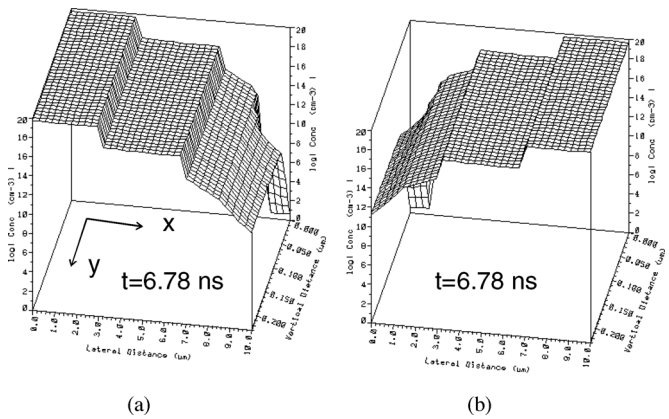

Fig. 3. 2-D (a) hole, and (b) electron concentration profiles at $t = 6.78$ ns under the forward biasing voltage at 0.89 V.

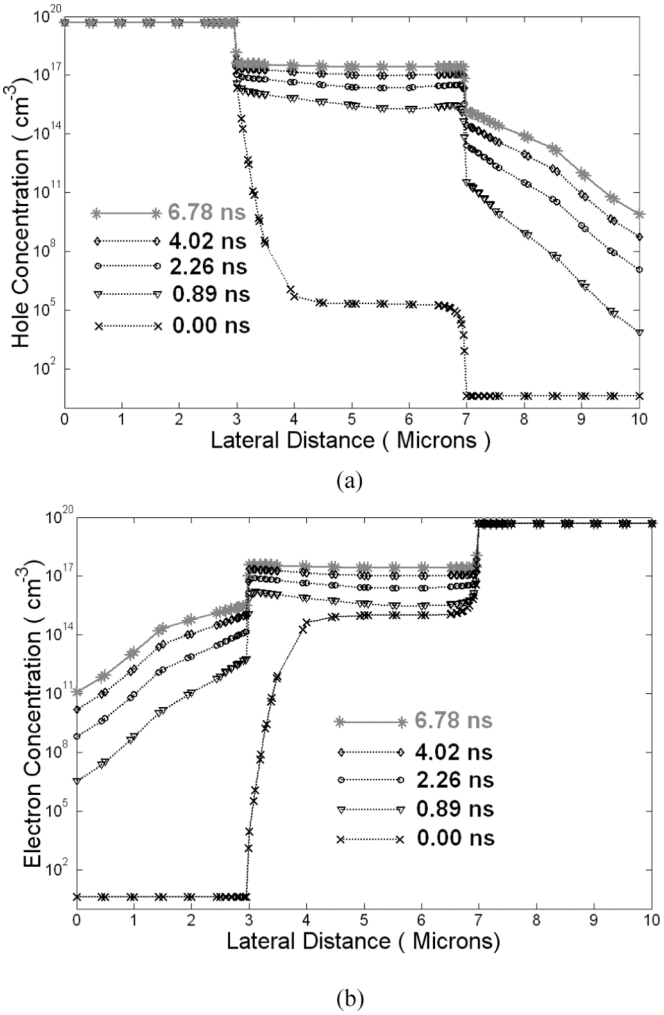

Fig. 4. Carrier concentration profiles at the half depth of the top silicon layer at various time points under the forward biasing voltage at 0.89 V. (a) Time-dependent hole concentration distribution. (b) Time-dependent electron concentration distribution.

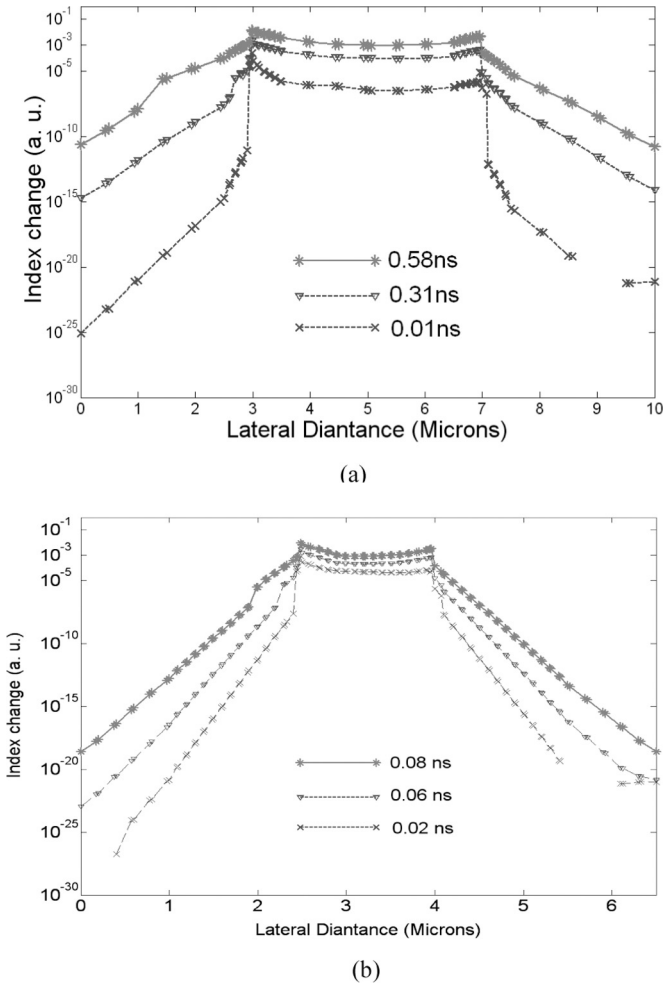

Fig. 5. Refractive index change along the lateral dimension of the p-i-n diode at the half depth of the top silicon layer under the forward biasing voltage at 2 V. (a) p-i-n diode with the intrinsic region of 4 μm. (b) p-i-n diode with the intrinsic region of 1.5 μm.

for gigahertz modulation. Recalling the discussion regarding the transit speed versus the current density in Section II, we have learned that the speed can be improved at a cost of higher current density. Given the fact that our devices are largely scaled down compared with the conventional devices, we are able to improve the speed by increasing the current density to a level such that the overall power consumption is still reasonably low for practical applications. A higher voltage of 2 V, which accordingly provides higher current density, is applied for the improvement of device speed. To obtain a more straightforward insight, variations of the free carrier concentration extracted from the simulation results were subsequently converted to the refractive index changes using (1). As is seen in Fig. 5(a), the targeted refractive index change of 0.001 (corresponding to an injection level of $3 \times 10^{17}\mathrm{cm}^{-3}$) has been reached within 0.58 ns under 2 V after switching on the p-i-n diode, which ensures the gigahertz modulation capability.

Reducing the width of the intrinsic region could be an efficient way to further increase the switching speed, whereas it may also cause extra optical loss depending on how large the overlap between the guided optical mode and the highly absorptive p^+ and n^+ regions is. Our earlier simulation revealed that the energy density drops by 20 dB at a distance of 0.75 μm away from the central line of PCW [22], which sets the lower limit of the separation distance between two highly doped regions at around 1.5 μm. The transient behavior of a 1.5-μm-wide p-i-n diode is simulated. Fig. 5(b) shows the corresponding time-dependent spatial change in the refractive index of the silicon core layer. A significant decrease in the carrier filling time is observed in this shrunk structure. Within 0.077 ns after turning on the device, a fairly uniform index change of 0.001 is attained over the entire intrinsic or waveguiding region. It gives another tenfold reduction of the switching speed from the 4-μm-wide device, pushing the modulation capability up to10 GHz. More importantly, with a given interaction length of a PC MZI, index changes smaller than 0.001 might be sufficient to ensure a complete switching function. It virtually depends on how much the enhancement of the group refractive index could be obtained in a specifically designed PC structure. In principle, an even faster switching speed can be achieved in a p-i-n-diode-embedded PC modulator if

deliberate efforts would be made in the band structure design of PCs.

IV. Experiments

Considering the complication of fabrication procedures, we built our silicon PC MZI modulator using the previously simulated 4-μm-wide structure. A wafer with the top silicon layer of 260 nm and a buried oxide layer of 2 μm was selected as the device substrate. A thermal oxide of about 80 nm, grown at 850 °C in H_2O atmosphere, served as an etching mask for silicon reactive ion etching (RIE). In addition, this thin oxide worked as a screen layer to minimize the channeling effect occurring in the ion implantation. The device structure using the previously simulated lattice parameters was defined by electron beam lithography. Device patterns were transferred to the oxide layer by RIE using CHF_3. The next step is to strip off the electron beam resist by a heated Pirahna (solution of sulfuric acid and hydrogen peroxide) cleaning. Following that, the device structure was defined on the silicon core layer by RIE to a depth of 230 nm using oxide as the hard mask. The windows for p^+ and n^+ implantation were opened by photolithography. Ion implantations of boron at 30 keV and phosphorus at 50 keV were performed to achieve an average doping concentration about 5×10^{19} cm^{-3} for highly doped p^+ and n^+ regions. The thermal rapid annealing for 1 m at 950° in a flowing nitrogen environment was performed afterwards to anneal the lattice defects and activate the implanted atoms. After that, electrode contact windows were opened by photolithography and the top thermal oxide inside the windows were removed. Aluminum electrodes were made by electron-beam evaporation and a subsequent lift-off process. Finally, a good ohmic contact between the aluminum electrodes and the underlying silicon was formed by sintering the device at a temperature of 400 °C for 30 min in a forming gas ambient. As the last step, an acrylate-based polymer layer was coated to cover the whole device. The microscopic image of the resulting device is shown in Fig. 6. To sustain high current density, care was taken to design the geometry of the highly doped regions and electrodes. For example, our initial experiments, in which the p^+ and n^+ regions in early fabricated samples were longer than the PCW, showed that the PC p-i-n diode tended to break down at the two ends of a PCW. This was identified to arise from highly concentrated electrical field, and the accompanying high electrical current density, localized at the PCW ends. Shortening p^+ and n^+ regions, as shown in Fig. 6, overcame this issue.

The I–V characteristic of the PC p-i-n diode was measured and the result is plotted in Fig. 7. Similar to the I–V dependence of the conventional p-i-n diode described by Shockley's and Hall's theories [24], the I–V relation $I \sim \exp(qV/k_BT)$ in the low-level injection region and $I \sim \exp(qV/2k_BT)$ in the high-level region are both observed, where V is the applied voltage, k_B is the Boltzmann's constant, and T is the temperature. This electrical characterization experimentally confirmed that the operation of our device, which was biased at 2 V for the turn-on state, run into a scenario of high-level current injection, where our theoretical analysis presented in Section IV is

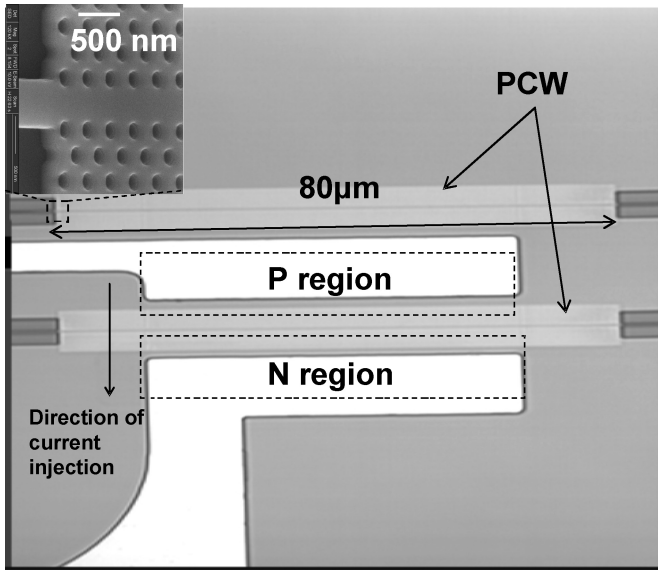

Fig. 6. Microscopic image of a p-i-n-diode-based PC MZI silicon modulator. The inset is the scanning electron microscopy image of the defect-line silicon PCW.

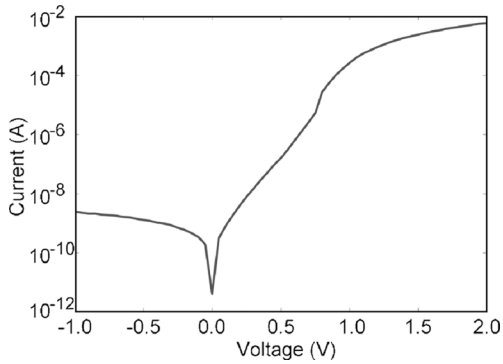

Fig. 7. I–V curve of the PC p-i-n.

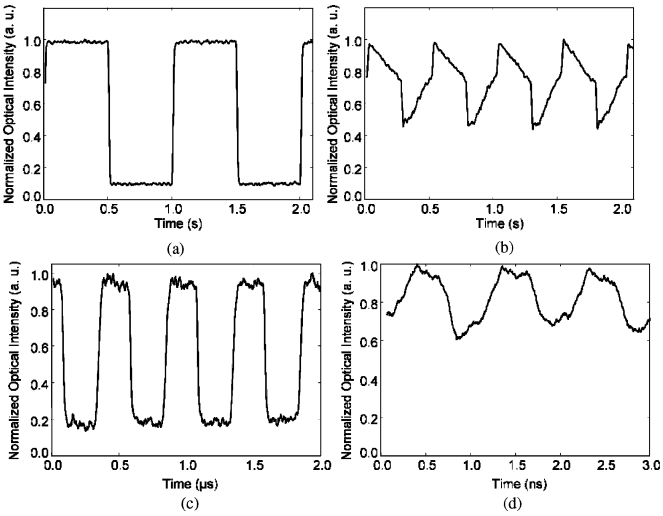

Fig. 8. Modulation traces at: (a) 1 Kb · s^{-1}. (b) 200 Kb · s^{-1}. (c) 2 Mb · s^{-1}. (d) 1 Gb · s^{-1}.

readily applied. We used TE-polarized light at a wavelength of 1541 nm, which is close to the transmission band edge of the defect mode, for the optical characterization. Lensed and tapered polarization maintaining fibers were used to couple the light into and out of the on-chip devices. An Agilent 8133 A pulse generator (up to 3 Gb $\cdot$ s^{-1}) was used to generate electrical driving signals. Modulated optical signals were detected by a 30-GHz photo detector that is internally integrated in the HP 83480 A digital communication analyzer. Square wave electrical signals at a peak-to-peak voltage of 3 V ($V_{\rm on} = 2$ V, $V_{\rm off} = -1$ V) with a duty cycle of 50% were used for the dynamic modulation characterization. Fig. 8 shows the optical modulation signals at various bit rates. It must be noted that the waveform of the modulated signal varies appreciably versus the modulation frequency. For the modulation at very low speed, the modulated signal reproduces the square wave of the driving signal perfectly, as shown in Fig. 8(a). A severe distortion of the waveform accompanied with the reduced modulation depth has been found in the modulated signal when the modulation speed increases to a few hundreds kilobits per second. Interestingly, good quality of modulation signals is regained when further increasing the modulation frequency up to a few megahertz. We believe that this phenomenon is related to the competition between the electrooptic and thermooptic effect that is inevitably involved in a current injection process. As current injection is always associated with power dissipation, the thermal effect of joule heating is always present in a current device. In contrast to the plasma effect, i.e., excess free carriers reduce the refractive index, temperature rise due to joule heating increases the refractive index. However, the thermal response is much slower than the electrical response. Typically, thermooptic effect cannot reach the frequency response beyond a few hundreds of kilohertz [28]. Consequently, it competes with the plasma dispersion effect in an opposite way for low-frequency modulations. The variation of the modulation trace versus frequency, shown in Fig. 8(a)–(d), delineates a clear transition from the thermal domination at low frequencies to plasma domination at high-frequency region. It is estimated that the temperature increase in our device under a forward operation is around 10°, which approximately leads to refractive index change of 0.002 in silicon. Therefore, the thermooptic effect dominates over the plasma effect at the low-frequency region. However, the thermal dominance starts getting weaker and weaker as the operation speed increases up to a few hundreds of kilohertz, the speed at which the thermal response can hardly keep pace with the electrical driving signal. An obvious degradation in the modulation at 200 Kb$\cdot$s^{-1}, a corner frequency of the thermal response region, has been observed, as shown in Fig. 8(b). As the frequency further increases to above a few megahertz, when the thermo-effect is no longer able to pick up such a fast switching speed, plasma effect starts to play a major role in the modulation mechanism. As is shown in Fig. 8(c), a square-wave modulation curve resembling the low-frequency signal appears when the frequency increases to 2 Mb $\cdot$ s^{-1}, which demonstrates the high-speed response of the electrooptic effect. Fig. 8(d) shows that the modulation depth is reduced by 3 dB as the modulation frequency further increases to 1 Gb $\cdot$ s^{-1}. The measured speed limit is in good agreement with the electrical simulation. To make electrooptic modulation more efficient, a good thermal heat sink has to be designed to minimize the competition from thermooptic effect. The demonstrated modulation above 2 Mb $\cdot$ s^{-1} is considered a pure electrooptic modulation. A reliable device performance at gigahertz operation frequency of our current device is readily achieved using especially designed high-speed drive circuitry. Further speed improvement can be achieved using the shrunk p-i-n diode we proposed earlier.

V. Conclusion

A p-i-n-diode-based PC silicon electrooptic MZI modulator has been proposed and fabricated. By incorporating PCWs into the MZI structure, device size has been reduced by more than one order of magnitude compared to the conventional devices. Optical simulation based on the plane-wave expansion method has been performed to reveal how slow group velocity in the silicon PCW dramatically increases the phase shift and thus reduces the size of the MZI modulator. We have performed electrical analyses to estimate device switching behavior by simulating time-dependent distributions of the carrier concentration. Simulations show that increasing current density under a given injection current by reducing the device size brings a huge speed advantage. The modulation capability above 10 GHz is predicted by shrinking the width of central intrinsic region of a p-i-n diode down to 1.5 μm. The high-speed electrooptic modulation at 1 Gb $\cdot$ s^{-1} has been experimentally demonstrated in a PC silicon MZI modulator within an interaction length of 80 μm. The inevitably involved thermooptic effect due to the high current injection is observed for modulations at low frequencies.

Acknowledgment

The devices were fabricated at UT Microelectronics Research Center.

References

[1] R. Soref, "Silicon photonics technology: Past, present, and future," *IEEE J. Sel. Topics Quantum Electron.*, vol. 12, no. 6, pp. 1678–1687, Nov./Dec. 2006.

[2] R. A. Soref and B. R. Bennett, "Electrooptical effects in silicon," *IEEE J. Quantum Electron.*, vol. QE-23, no. 1, pp. 123–129, Jan. 1987.

[3] G. V. Treyz, P. G. May, and J.-M. Halbout, "Silicon Mach–Zehnder waveguide interferometers based on the plasma dispersion effect," *Appl. Phys. Lett.*, vol. 59, pp. 77–773, 1991.

[4] C. Z. Zhao, G. Z. Li, E. K. Liu, Y. Gao, and X. D. Liu, "Silicon on insulator Mach–Zehnder waveguide interferometers operating at 1.3 μm," *Appl. Phys. Lett.*, vol. 67, pp. 2448–2451, 1995.

[5] P. Dainesi, A. Kung, M. Chabloz, A. Lagos, Ph. Fluckiger, A. Ionescu, P. Fazan, M. Declerq, Ph. Renaud, and Ph. Robert, "CMOS compatible fully integrated Mach–Zehnder interferometer in SOI technology," *Photon. Technol. Lett.*, vol. 12, no. 6, pp. 660–662, Jun. 2000.

[6] A. Liu, R. Jones, L. Liao, D. S. Rublo, D. Rubin, O. Cohen, R. Nicolaescu, and M. Paniccia, "A high-speed silicon optical modulator based on a metal-oxide-semiconductor capacitor," *Nature*, vol. 427, pp. 615–617, 2004.

[7] L. Liao, D. Samara-Rubio, M. Morse, A. Liu, D. Hodge, D. Rubin, U. D. Keil, and T. Franck, "High speed silicon Mach–Zehnder modulator," *Opt. Exp.*, vol. 13, pp. 3129–3135, 2005.

[8] L. Gu, W. Jiang, X. Chen, L. Wang, and R. T. Chen, "High speed silicon photonic crystal waveguide modulator for low voltage operation," *Appl. Phys. Lett.*, vol. 90, pp. 071105-1–071105-3, 2007.

[9] A. Cutolo, M. Iodice, P. Spirito, and L. Zeni, "Silicon electro-optic modulator based on a three terminal device integrated in a low-loss single-mode SOI waveguide," *J. Lightw. Technol.*, vol. 15, no. 3, pp. 505–518, Mar. 1997.
[10] A. Irace, G. Breglio, and A. Cutolo, "All-silicon optoelectronic modulator with 1 GHz switching capability," *Electron. Lett.*, vol. 39, pp. 232–233, 2003.
[11] C. E. Png, S. P. Chan, S. T. Lim, and G. T. Reed, "Optical phase modulator for MHz and GHz modulation in silicon-on-insulator (SOI)," *J. Lightw. Technol.*, vol. 22, no. 6, pp. 1573–1582, Jun. 2004.
[12] F. Gan and F. X. Kartner, "High-speed silicon electrooptic modulator design," *IEEE Photon. Technol. Lett.*, vol. 17, no. 5, pp. 1007–1009, May 2005.
[13] F. Y. Gardes, G. T. Reed, and N. G. Emerson, "A sub-micron depletion-type photonic modulator in silicon on insulator," *Opt. Exp.*, vol. 13, pp. 8845–8853, 2005.
[14] Y. A. Vlasov, M. O'Boyle, H. F. Hamann, and S. J. McNab, "Active control of slow light on a chip with photonic crystal waveguides," *Nature*, vol. 438, pp. 65–69, 2005.
[15] Y. Jiang, W. Jiang, L. Gu, X. Chen, and R. T. Chen, "80-micron interaction length silicon photonic crystal waveguide modulator," *Appl. Phys. Lett.*, vol. 87, pp. 221105-1–221105-2, 2005.
[16] W. Jiang, L. Gu, X. Chen, and R. T. Chen, "Photonic crystal waveguide modulators for silicon photonics: Device physics and some recent progress," *Solid-State Electron.*, vol. 51, pp. 1278–1286, 2007.
[17] J. D. Joannopoulos, R. D. Meade, and J. Winn, *Photonic Crystals*. Princeton, NJ: Princeton Univ. Press, 1995.
[18] M. Notomi, K. Yamada, A. Shinya, J. Takahashi, C. Takahashi, and I. Yokohama, "Extremely large group-velocity dispersion of line-defect waveguides in photonic crystal slabs," *Phys. Rev. Lett.*, vol. 87, pp. 253902-1–253902-4, 2001.
[19] M. Soljacic, S. G. Johson, S. Fan, M. Ibanescu, E. Ippen, and J. D. Joannopoulos, "Photonic-crystal slow-light enhancement of nonlinear phase sensitivity," *J. Opt. Soc. Amer. B*, vol. 19, pp. 2052–2059, 2002.
[20] T. Baba, A. Motegi, T. Iwai, N. Fukaya, Y. Watanabe, and A. Sakai, "Light propagation characteristics of straight single-line-defect waveguides in photonic crystal slabs fabricated into a silicon-on-insulator substrate," *IEEE J. Quantum Electron.*, vol. 38, no. 7, pp. 743–752, Jul. 2002.
[21] M. L. Povinelli, S. G. Johnson, and J. D. Joannopoulos, "Slow-light, band-edge waveguides for tunable time delays," *Opt. Exp.*, vol. 13, pp. 7145–7159, 2005.
[22] L. Gu, Y. Jiang, W. Jiang, X. Chen, and R. T. Chen, "Silicon-on-insulator-based photonic-crystal Mach–Zehnder interferometers," *Proc. SPIE*, vol. 6128, pp. 261–268, 2006.
[23] X. Ghandi, *Semiconductor Power Devices*. New York: Wiley, 1977.
[24] A. Herlet, "The forward characteristic of silicon power rectifiers at high current densities," *Solid-State Electron.*, vol. 11, pp. 717–742, 1968.
[25] C. A. Barrios, V. Almeida, and M. Lipson, "Low-power-consumption short-length and high-modulation-depth silicon eletrooptic modulator," *J. Lightw. Technol.*, vol. 21, no. 4, pp. 1089–1098, Apr. 2003.
[26] J. Muller, "Thin silicon film p-i-n photodiodes with internal reflection," *IEEE J. Solid-State Circuts*, vol. SSC-13, no. 1, pp. 173–179, Feb. 1978.
[27] *MEDICI User's Manual*, TMA Inc., Palo Alto, CA, 1992.
[28] G. Cocorullo, M. Iodice, I. Rendina, and P. M. Sarro, "Silicon thermo-optical micro-modulator with 700 kHz-3 dB bandwidth," *IEEE Photon. Technol. Lett.*, vol. 7, no. 4, pp. 363–365, Apr. 1995.

Lanlan Gu received the B.S. and M.S. degrees in physics from Fudan University, Shanghai, China, in 1998, and 2001, respectively, and the Ph.D. degree in electrical and computer engineering from the University of Texas, Austin, in 2007.

She is currently a Research Scientist with Omega Optics, Inc., where she is involved in electrooptic laser beam steering and light emitting devices. Her current research interests include a variety of topics in the areas of optical communications and optical interconnects, which extend from free-space diffractive optical elements to integrated photonic devices. She has authored or coauthored over 40 publications in refereed journals and conferences.

Wei Jiang received the B.S. degree in physics from Nanjing University, Nanjing, China, in 1996, and the M.A. degree in physics and the Ph.D. degree in electrical and computer engineering from the University of Texas, Austin, in 2000 and 2005, respectively.

Since 2007, he has been an Assistant Professor in the Department of Electrical and Computer Engineering, Rutgers University, Piscataway, NJ. His current research interests include the intersection of nanotechnology and photonics with current emphasis on photonic crystals, silicon photonics, optical interconnects, and beam steering.

Xiaonan Chen received the B.S. degree in precision instruments and mechanology from Tsinghua University, Beijing, China, in 2002, and the M.S. degree in electrical and computer engineering from the University of Texas, Austin, in 2006, where he is currently working toward the Ph.D. degree at the Microelectronics Research Center.

Ray T. Chen (M'91–SM'98–F'04) received the B.S. degree in physics from the National Tsing-Hua University, Hsinchu, Taiwan, in 1980, and the M.S. degree in physics and the Ph.D. degree in electrical engineering from the University of California (UC), Berkeley, in 1983 and 1988, respectively.

From 1988 to 1992, he was a Research Scientist, a Manager, and the Director of the Department of Electrooptic Engineering, Physical Optics Corporation, Torrance, CA. During 1992, he was engaged to start optical interconnect research program as a Faculty Member in the Department of Electrical and Computer Engineering (ECE), University of Texas (UT), Austin, where his group reported its research findings in more than 420 published papers including over 55 invited papers. He holds 12 issued patents. His current research interests include nanophotonic passive and active devices for optical interconnect applications, polymer-based guided wave optical interconnection and packaging, and true time delay (TTD) wideband phased array antenna (PAA). He has edited or coedited over 18 conference proceedings.

Dr. Chen is a Fellow of the Optical Society of America (OSA) and the International Society for Optical Engineers (SPIE). He was the recipient of the 1987 UC Regent's Dissertation Fellowship and the 1999 UT Engineering Foundation Faculty Award for his contributions in research, teaching, and services.